Available online at www.sciencedirect.com
ScienceDirect
Trans. Nonferrous Met. Soc. China 35(2025) 1919−1936
Transactions of Nonferrous Metals Society of China
www.tnmsc.cn

Effect of sulfate-reducing bacteria on corrosion of copper and brass

Shu-hua XU[1], Qin WANG[1], Zhuo-wei TAN[1], Xiao-bao ZHOU[1], Cong LI[1], Zhen-sheng WANG[2], Tang-qing WU[1]

1. School of Materials Science and Engineering, Xiangtan University, Xiangtan 411105, China;
2. School of Mechanical Engineering, Hunan University of Science and Technology, Xiangtan 411105, China

Received 13 October 2023; accepted 9 May 2024

Abstract: The sulfate-reducing bacteria (SRB) corrosion of H70 brass, H80 brass and T2 copper was systematically studied using microstructure characterizations and electrochemical measurements. The results showed that H70 brass, H80 brass and T2 copper exhibited good corrosion resistance in the sterile environment, and the corrosion products were mainly metal oxides, such as Cu_2O, CuO and ZnO. The SRB metabolism sharply accelerated the corrosion process of three types of copper alloys, especially the T2 copper. In the inoculated environment, an additional mixture of Cu_2S, ZnS and $CuSO_4$ existed in the corrosion products. Pitting corrosion was the main corrosion style for the H70 brass and H80 brass, while general corrosion and pitting corrosion simultaneously dominated the corrosion process of the T2 copper in this environment. The results provide a new insight to the microbiological corrosion of copper alloys.
Key words: copper; brass; sulfate reducing bacteria; microbiologically influenced corrosion; microstructure

1 Introduction

Corrosion is taking place for almost all metals serving in natural and industrial environments, causing severe safety accidents and huge economic loss throughout the world [1]. It is reported that the economic loss caused by corrosion failure accounts for 1%−5% of the gross national product (GNP) [2], of which micro- biologically influenced corrosion (MIC) accounts for about one-fifth [3]. Under specific conditions, microorganisms accelerate the corrosion process of metals by the means of adsorption, penetration and secretion, eventually leading to the failure of metal construction [4−6]. Sulfate-reducing bacteria (SRB), nitrate-reducing bacteria (NRB), acid-producing bacteria (APB) and iron-oxidizing bacteria (IOB) are the well acknowledged microorganisms involving in MIC. Among them, SRB could obtain electrons from organic carbon source or high energy metal directly for cell respiration [7−10]. Thus, SRB corrosion is one of the most common in anaerobic environment [11]. The investigations on the behavior and mechanism of SRB corrosion are gaining the attention of the engineers and scientists all over the world [12,13]. Currently, the widely recognized mechanisms of SRB corrosion include but are not limited to cathode depolarization theory (CDT), concentration cell theory [14], metabolite corrosion theory [15], biocatalytic cathodic sulfate reduction (BCSR) theory [16] and extracellular electron transfer (EET) theory [17,18].

Copper and its alloys are widely used in our living and industrial environments due to their good electrical conductivity, high thermal stability and high corrosion resistance [19]. During the initial stage of the service of the copper and its alloys, a protective Cu_2O film could form on their surfaces, which could protect the matrix from corrosion. Although copper and its alloys show high corrosion resistance, corrosion degradation, especially MIC,

Corresponding author: Tang-qing WU, Tel: +86-13875256157, E-mail: tqwu10s@alum.imr.ac.cn, tqwu@xtu.edu.cn
https://doi.org/10.1016/S1003-6326(25)66791-4

could still occur [20,21]. HUTTUNEN et al [22] found that SRB physiological activities altered the chemical properties of the groundwater and the local conditions of the metal surface, and greatly promoted the corrosion rate of T2 copper. According to the results of DOU et al [23,24], under the action of the SRB physiological activities, the corrosion rate of T2 copper is much greater than that of carbon steel. The above results indicate that T2 copper is sensitive to MIC corrosion.

Brass is a kind of copper alloys composed of copper and zinc. H70 and H80 brasses, which are single-phase alloys, are the typical representatives of brass. Microbial activities in natural seawater could lead to an increase in corrosion products on the brass surface and a higher corrosion rate of the brass matrix [25]. ZHAO et al [26] noted that both *Pseudomonas aeruginosa* and *Desulfovibrio desulfuricans* (*D. desulfuricans*) could promote the corrosion process of brass, in which the biofilm played a crucial role. Therefore, it is evident that the MIC of copper and brass has garnered scholarly attention worldwide. However, the MIC mechanism of brass remains unclear, and the differences in MIC behavior between brass and copper are not yet acknowledged.

In this work, the corrosion behavior of H70 brass, H80 brass and T2 copper in sterile and inoculated ATCC1249 medium was systematically studied by scanning electron microscope with energy disperse spectroscopy (SEM−EDS), 3D ultra-depth microscope, electrochemical measurement and X-ray photoelectron spectroscopy (XPS). The differences in MIC pattern of the three types of metals were revealed, and the corresponding corrosion mechanism was discussed.

2 Experimental

2.1 Samples and bacteria

The materials used in this experiment were H70 brass, H80 brass and T2 copper. The chemical composition (wt.%) of H70 brass was Cu 70.91, Zn 29.06, Ni 0.03, and that of H80 brass was Cu 82.6, Zn 17.38, and Ni 0.02. The chemical composition (wt.%) of T2 copper was Cu 99.99. The materials were separated by wire cutting into 10 mm × 10 mm × 5 mm and 30 mm × 20 mm × 5 mm. A copper wire was spot-welded on the back of the sample with size of 10 mm × 10 mm × 5 mm, and all non-working surfaces of this type of samples were covered with epoxy resin. The samples were used for electrochemical measurement. The samples with size of 30 mm × 20 mm × 5 mm were used for mass loss and morphology analysis. All working surfaces of the samples were ground and polished successively with alumina sandpaper (280, 400, and 800 grids) and silicon carbide sandpaper (600, 800, and 1200 grids), cleaned with distilled water and anhydrous ethanol, and dried by cold air. Before the experiment, all samples were placed in an anaerobic glove box and irradiated with ultraviolet radiation, to avoid bacterial contamination.

The SRB strain (*D. desulfuricans*, CGMCC 1.5189) was selected from China General Microbial Culture Collection Center. Prior to the experiment, *D. desulfuricans* was activated in API RP-38 medium for more than 3 generations, and the SRB strains with high physiological activity were used in the subsequent experiments. API RP-38 medium contains (g/L) $MgSO_4·7H_2O$ 0.2, ascorbic acid 1.0, NaCl 10, KH_2PO_4 0.5, sodium lactate 4.0, yeast paste 1.0, and Fe $(NH_4)_2(SO_4)_2$ 0.02. The pH values of the mediums were adjusted to be 7.0−7.2.

2.2 Experimental solution and procedure

The ATCC1249 medium was selected as the experimental medium. 1 L of ATCC1249 medium contains the following components: 2.0 g $MgSO_4$, 5.0 g $Na_3C_6H_5O_7$, 1.0 g $CaSO_4·2H_2O$, and 1.0 g NH_4Cl, 1000 mL distilled water, 0.5 g K_2HPO_4, 3.5 g $NaC_3H_5O_3$, 1.0 g yeast extract, and 1.0 g $(NH_4)_2Fe(SO_4)_2$. The experiment was conducted using a freshly prepared medium that had been deoxygenated with pure N_2 for 2 h and sterilized in an autoclave at 121 °C for 30 min.

The deoxidized and sterile ATCC1249 medium was cooled to room temperature and inoculated with 1% SRB strain, which was deoxygenated with pure N_2 for 2 h and sealed with silicone plug. All of the above operations were carried out in a sterile and anaerobic glove box. Subsequently, the bottles were placed in a thermostatic container with temperature of (30±2) °C for 336 h. Bacterial counts and electrochemical measurements were performed at regular intervals during the experiment. After the experiment, the samples for mass loss and corrosion morphology were taken out

from the bottles. In this work, the media with and without *D. desulfuricans* were named as the inoculated medium and the sterile medium, respectively.

2.3 Bacteria counting

The amounts of the planktonic and sessile cells were determined using KBC-SRB culture flask (Zhengzhou Watt Detection Technology Co., Ltd.) according to the most probable number (MPN, GB/T14643.5—2009) method. After the experiment, the biofilm on the sample surfaces was collected for the amount counting of the sessile cells using the similar MPN method. The above operations followed the standard GB/T12998—1991.

2.4 Mass loss analysis

The initial mass (m_1) of the samples for the mass loss was recorded using an electronic analytical balance (LICHEN, FA324C). After the experiment, the corrosion products on their surfaces were removed using rust remover under the help of ultrasonic device. Then, these samples were successively washed with distilled water and anhydrous ethanol, and dried by cold air. The final mass (m_0) of the samples were recorded using the same balance. The rust remover was prepared according to the standard GB/T16545 — 2015, which was composed of 50 g aminosulfonic acid and 1 L distilled water. To ensure accuracy, three parallel samples were used for the experiment, and each sample was weighed more than two times until the mass error was within ±0.2 mg. The corrosion rate (R_c) of the samples was calculated as follows:

$$R_c = \frac{87600 \times (m_1 - m_0)}{\rho t A} \quad (1)$$

where ρ, t and A represent the density, immersed time and exposed area of the samples, respectively.

2.5 Characterization of microstructure and composition

After taking out from the bottles, the samples were immersed in glutaraldehyde (5.0 wt.%) for 5 h to fix the biofilm. Then, the samples were progressively dehydrated with 25, 50, 75 and 100 vol.% ethanol, and dried with pure N_2. The binding states of Cu 2p, S 2p and Zn 2p of the corrosion products on the sample surfaces were characterized by XPS (Thermo K-alpha, ESCALAB250XI). The XPS results were calibrated by C 1s sub-peaks of 284.6 eV and fitted with XPSPEAK 4.1 software package. The corrosion products and biofilms on the sample surfaces were observed using SEM (Zeiss EVO MA10) and EDS (Oxford X-MaxN). Then, the corrosion products on the sample surfaces were removed by the same rust removal. The corrosion morphology of the samples was observed by SEM, and the corrosion depth and width were measured by 3D digital microscopy (VHX−2000, Keyence).

2.6 Electrochemical measurement

Electrochemical measurements were carried out using an electrochemical workstation (Zahner Ennium, Germany). A common three-electrode system was selected, in which saturated calomel electrode (SCE) was used as reference electrode and platinum electrode as auxiliary electrode. The open circuit potentials (OCPs) of the samples were measured, following by the electrochemical impedance spectroscopy (EIS), and polarization curve were tested. EIS measurement was carried out at OCP, and the frequency ranged from 5 mHz to 100 kHz and the voltage amplitude of the sinusoidal signal was 10 mV. The scan rate of the polarization curves was 0.5 mV/s and its scan range was ±250 mV (vs OCP). Origin and Zsimpwin software packages were used to fit polarization curve and EIS, respectively. All experiments were repeated at least two times.

3 Results

3.1 Microstructure of brass and copper

The metallographic structures and EDS results of the H70 brass, H80 brass and T2 copper are shown in Fig. 1. The main phase of the H70 brass and H80 brass was the copper solid solution with zinc dissolution in it, which was named as (Cu, Zn) phase. The solid solution with relatively high zinc content dissolved during the corrosion step of the metallographic preparation, forming black corrosion pits embedding in the matrix (Figs. 1(a, b)) [27]. The metallographic grain of T2 copper polygonally shaped, and the equiaxed grains, deformed grains and typical twins constituted the general feature of its microstructure (Fig. 1(c)).

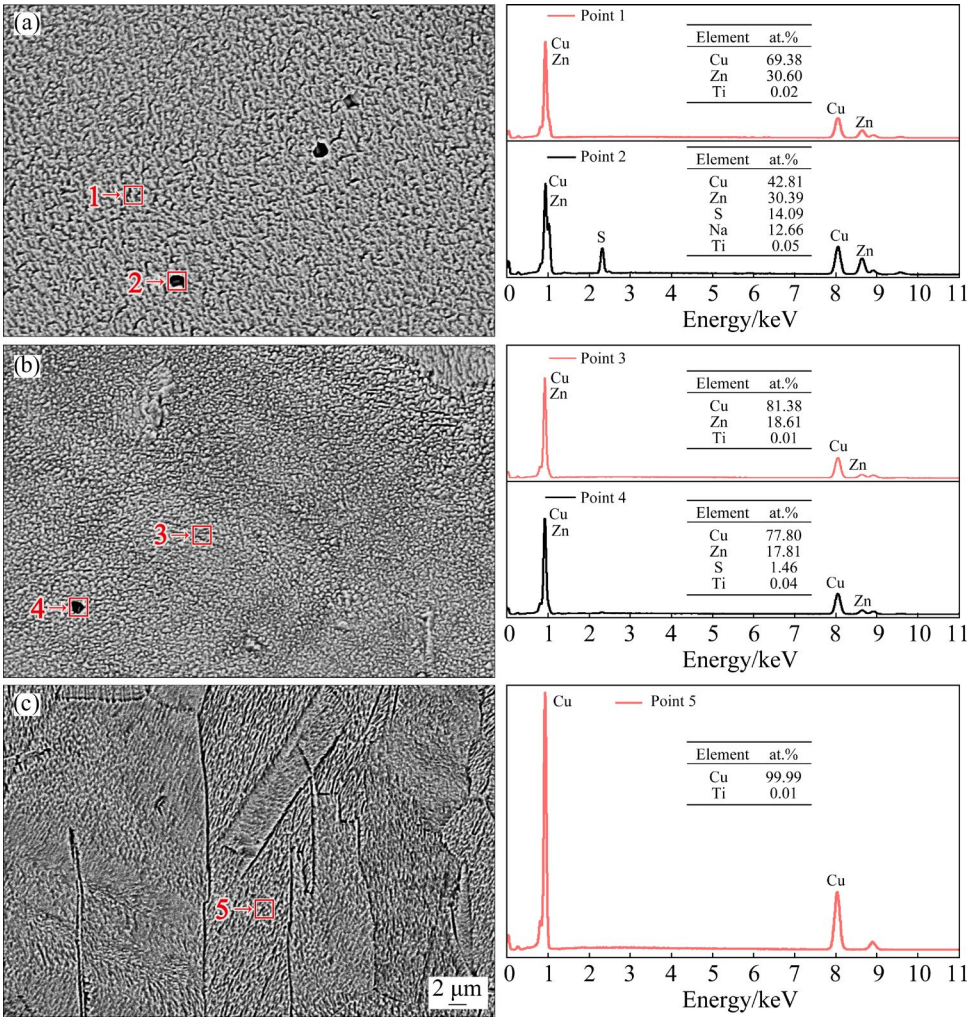

Fig. 1 Microstructures and EDS results of H70 brass (a), H80 brass (b), and T2 copper (c)

3.2 Bacterial growth and corrosion rate

Figure 2 shows the amount evolution of the planktonic SRB cells in the inoculated medium and the amount of the sessile cells on the surfaces of the three types of the samples after the experiment. In the inoculated medium, the amount evolution of the planktonic cells displayed a typical growth pattern in a closed container (Fig. 2(a)). During the initial stage of the experiment, SRB cells exponentially grew. At 72 h, they reached a peak of 9.5×10^9 cell/mL, after which they began to sharply decrease. At the end of the experiment, the amount of the planktonic cells kept at 2×10^5 cell/mL. The survival amount of the planktonic cells at this stage was only one ten-thousandth of the peak.

After 336 h of immersion, the amount of the sessile cells on the surfaces of H70 brass, H80 brass and T2 copper was 2×10^7, 2×10^8 and 2.8×10^{15} cell/cm^2, respectively (Fig. 2(b)). The amount of the sessile cells on the T2 copper surface was much higher than these on the surfaces of H70 brass and H80 brass. Besides, with the increase of copper content in the metal matrix, the amount of the sessile cells on the metal surface increased.

Figure 3 shows the corrosion rates of the three types of the samples after 336 h of immersion in the sterile and inoculated mediums. The corrosion rate of three types of the samples in the sterile medium was arranged in the range of 2−3 μm/a. The corrosion rates were very low and the difference between them was very little. In the inoculated medium with *D. desulfuricans*, the corrosion rate of the three types of copper alloys increased significantly. Among them, the corrosion rate of the T2 copper reached 249 μm/a, showing the most significant acceleration role of the SRB metabolism in corrosion process. Interestingly, the increasing trend of corrosion rates of three types of copper alloys

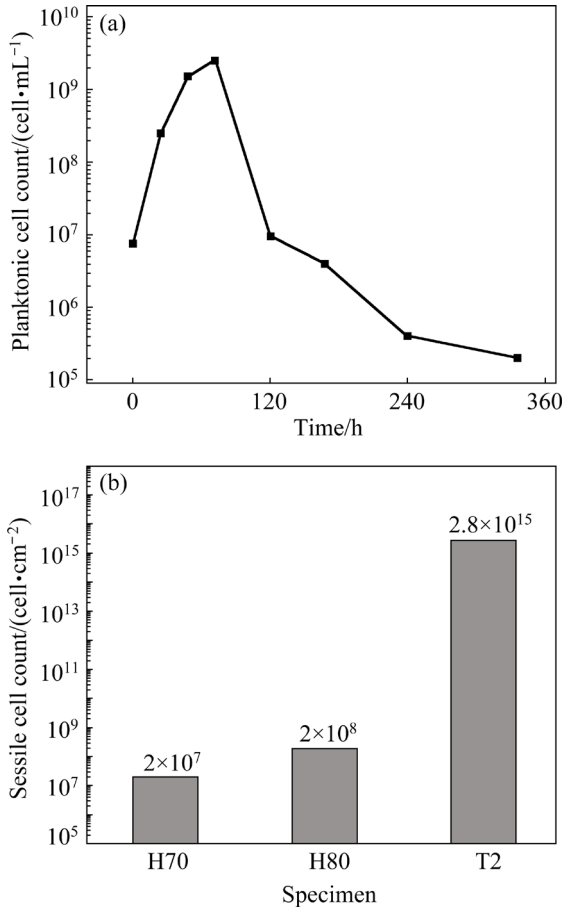

Fig. 2 Amount evolution of planktonic SRB cells in inoculated medium (a), and amount of sessile cells on surfaces of three types of samples after 336 h of immersion in inoculated medium (b)

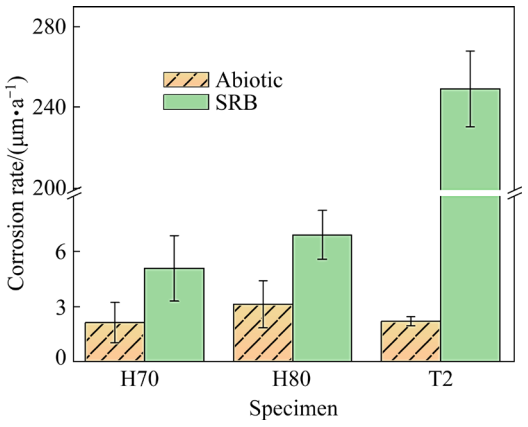

Fig. 3 Corrosion rates of brass and copper after 336 h of immersion in sterile and inoculated media

was consistent with the amount of sessile cells on sample surfaces (Fig. 2(b)). From the above results, it was discovered that SRB cells accelerated the corrosion process by attaching to the metal surface [28].

3.3 Corrosion products on brass and copper surfaces

The morphology of the corrosion products on the surface of the three types of copper alloys after 336 h of immersion in the sterile and inoculated mediums is shown in Fig. 4. All sample surfaces were covered by a layer of complete corrosion products, with noticeable delamination. The surfaces of the three types of copper alloys showed clear polish scratches in the sterile medium. The corrosion products were relatively less, indicating that the corrosion rates of the samples were low (Figs. 4(a, c, e)), which was consistent with the results of the corrosion rate (Fig. 3). In the inoculated medium, with the increase of the copper content in the sample matrix, the amount of the flocculent and nubbly corrosion products increased greatly (Figs. 4(b, d, f)).

The points marked by red letters in Fig. 4 are EDS detection points, and the corresponding EDS results are shown in Fig. 5. The corrosion products on the sample surfaces in the sterile medium were primarily composed of Cu, Zn, C, and O elements. This suggested that the corrosion products on the surfaces may be the oxides of Cu and Zn [29−31]. The content of Cu or Zn in the inner layer of the corrosion products was higher than that in outer layer, while that of element O was opposite (Figs. 5(a, c, e)). The facts indicated that much of the oxide existed in the outer layer. Compared with the results in the sterile medium, an additional element S was detected in the corrosion products on the sample surface in the inoculated medium, and the content of element S on the sample surface increased with the increase of the copper content in the sample matrix (Figs. 5(b, d, f)). As shown in Fig. 2, the amount evolution of the sessile cells on the metal surface was identical to the content evolution of element S in the corrosion products. One could reasonably assume that, the preferential attachment of *D. desulfuricans* cells to the surface of the sample with high Cu content might be relative to the formation of the sulfides in the corrosion products [32]. The XPS results of the corrosion products are shown in Fig. 6. The corrosion products on the sample surface in the sterile medium were primarily Cu_2O, CuO, and ZnO. However, in the inoculated medium, additional sulfur-containing compounds, such as Cu_2S, ZnS, and $CuSO_4$, were generated in the corrosion

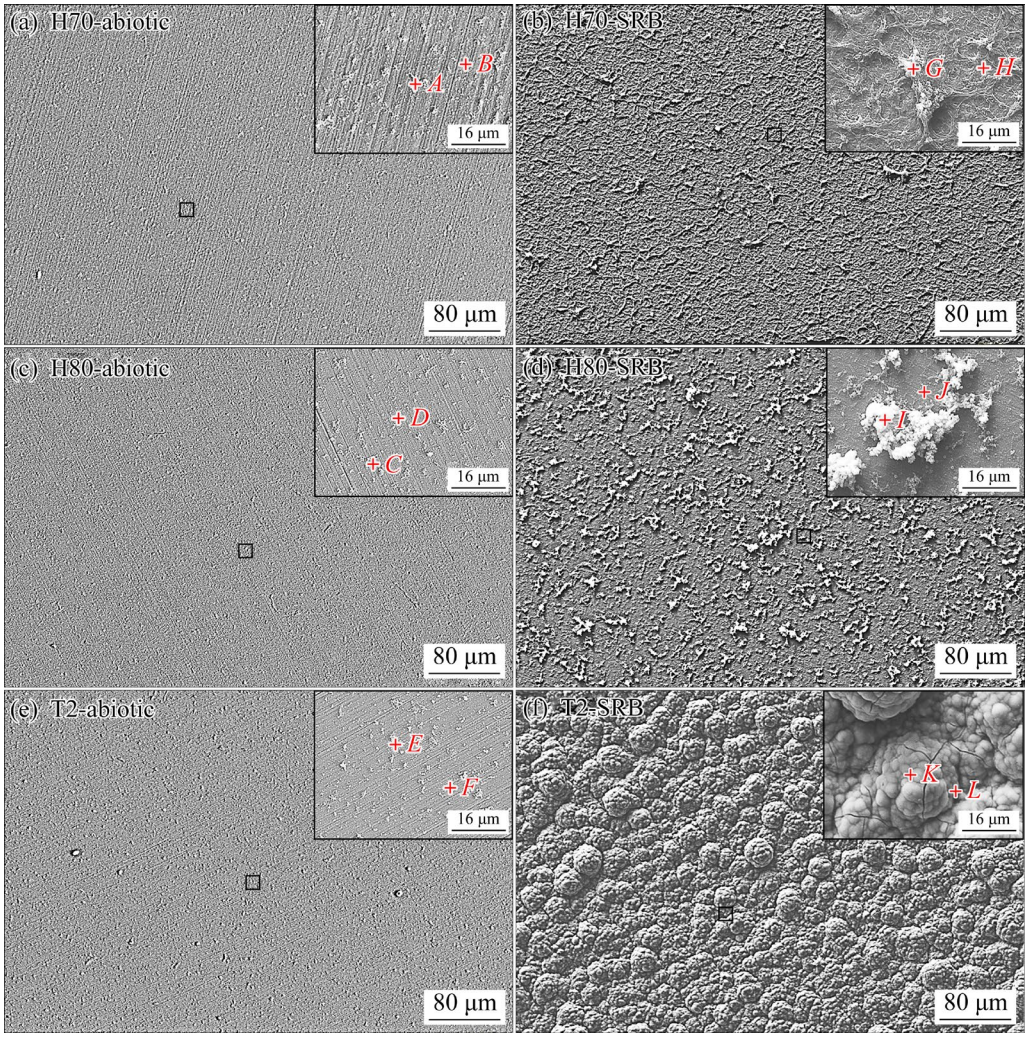

Fig. 4 Morphology of corrosion products on surface of brass and copper after 336 h of immersion in sterile (a, c, e) and inoculated (b, d, f) media: (a, b) H70; (c, d) H80; (e, f) T2

products, which was consistent with the EDS results (Fig. 5).

3.4 Corrosion morphology of brass and copper

Figure 7 shows the corrosion morphology of the three types of copper alloys after 336 h of immersion in the sterile and inoculated media. The polish scratches on the surface of the three samples were clearly visible in the sterile environment, reflecting the low corrosion rate of the three types of copper alloys in this environment, which was consistent with the result of corrosion rate (Fig. 3). There was no obvious corrosion pit formed on the surface of the T2 copper, but a few low-shallow corrosion pits generated on the surface of the H70 brass and H80 brass. As compared with Fig. 1, one can get that these low-shallow corrosion pits may be derived from the dissolution of the solid solution with relatively high zinc content on the sample surface. In the inoculated medium, the number and the diameter of corrosion pits on the surface of the three types of copper alloys increased significantly. The facts manifested that *D. desulfuricans* cells participated and accelerated the corrosion process of the alloys. With the increase of Cu content in the sample matrix, the number and diameter of corrosion pits increased dramatically. In addition, although large corrosion pits existed on the surface of T2 copper in the inoculated medium, there was no obvious polish scratch on this surface. The above results displayed that the more serious general corrosion and pitting corrosion simultaneously occurred on the surface of the T2 copper.

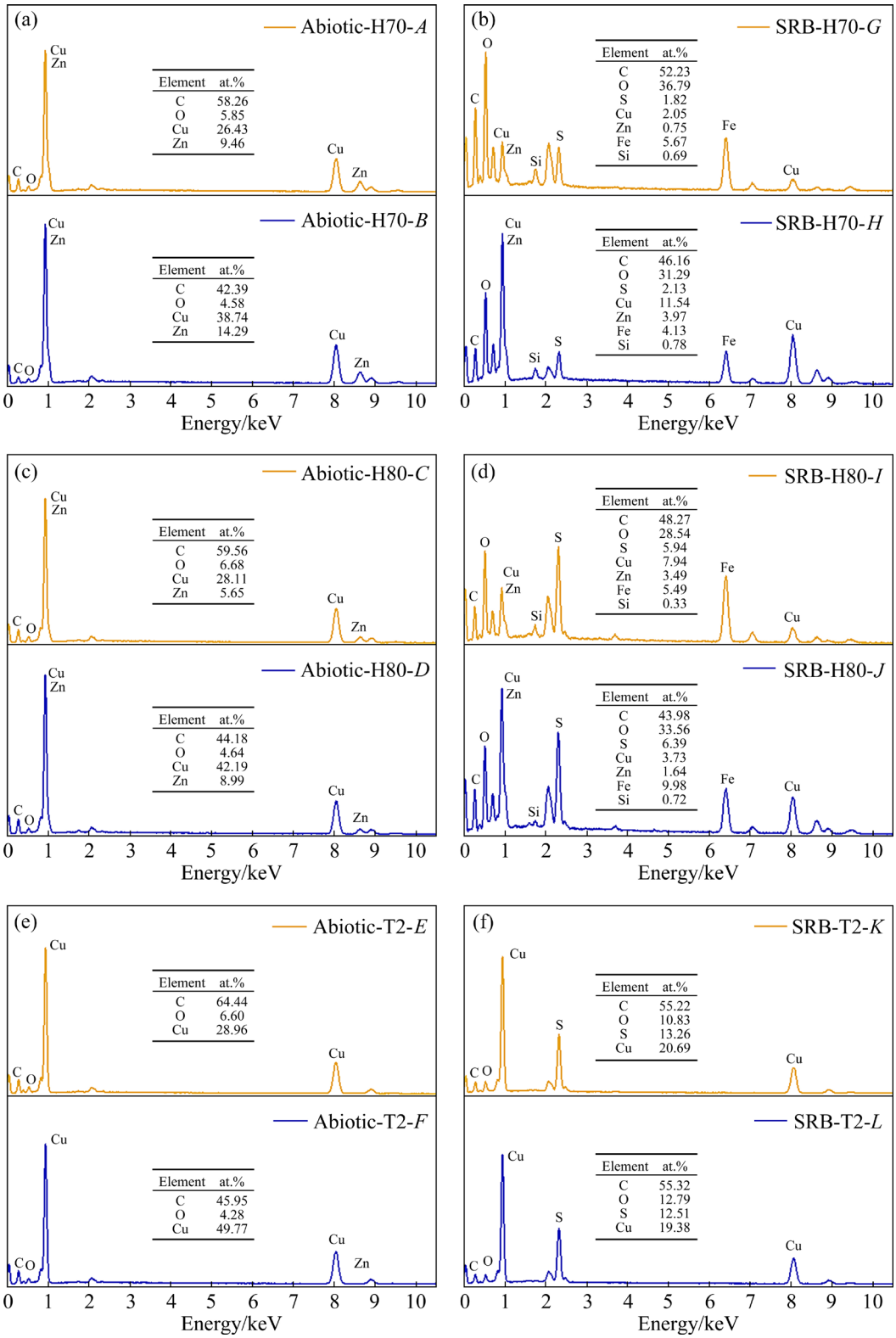

Fig. 5 EDS results of corrosion products on surface of brass and copper after 336 h of immersion in sterile (a, c, e) and inoculated (b, d, f) media: (a, b) H70; (c, d) H80; (e, f) T2 (*A*−*L* are shown in Fig. 4)

Figure 8 shows the 3D morphology of the sample surfaces after 336 h of immersion in the sterile and inoculated media. In the sterile medium, the maximum depths of the corrosion pits on the surfaces of the three types of copper alloys arranged in the range of 3−4 μm, which was very shallow. In the inoculated medium, the maximum depths of the corrosion pits on the surfaces of the H70 brass, H80

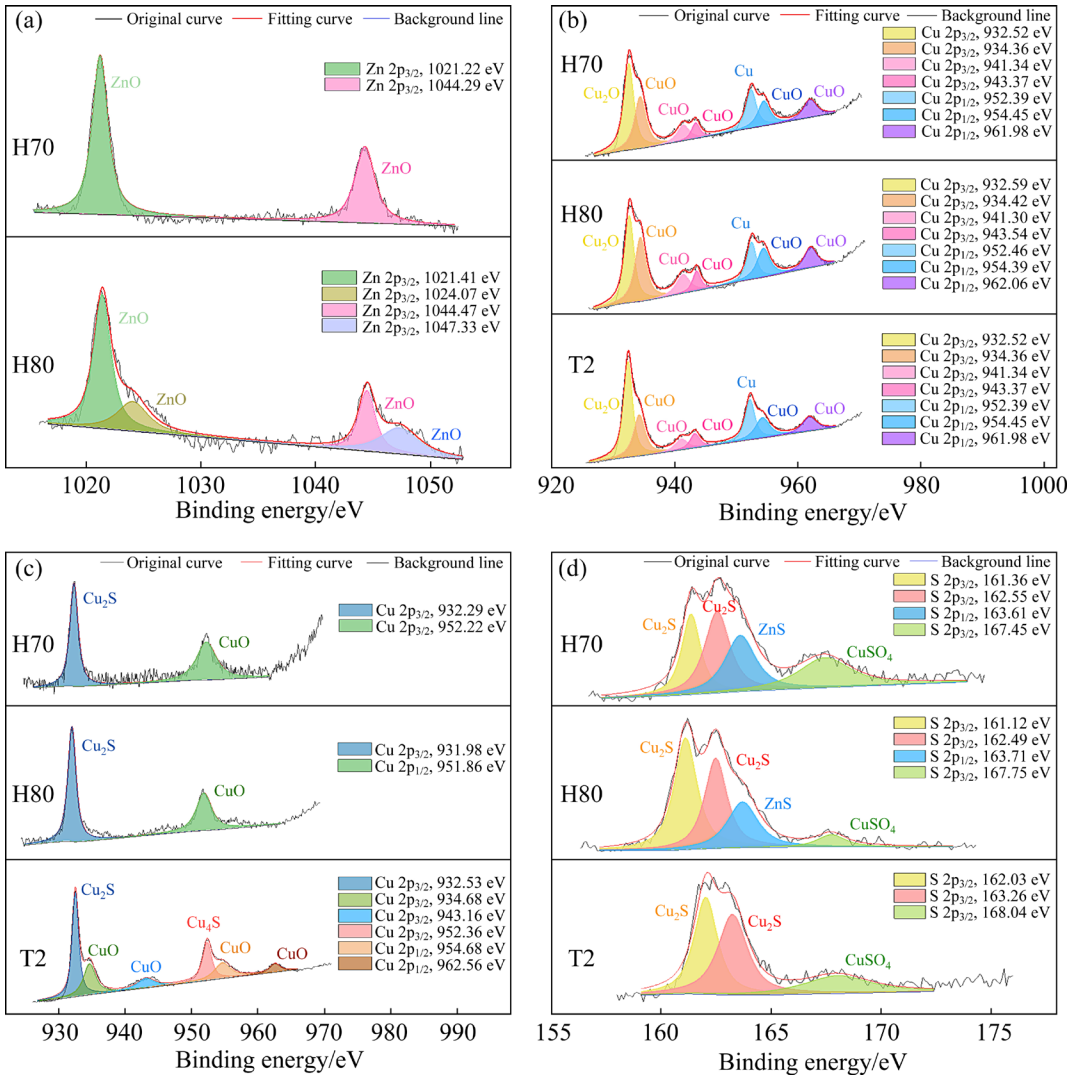

Fig. 6 XPS spectra of corrosion products on surface of brass and copper after 336 h of immersion in sterile (a, b) and inoculated (c, d) media: (a) Zn 2p; (b, c) Cu 2p; (d) S 2p

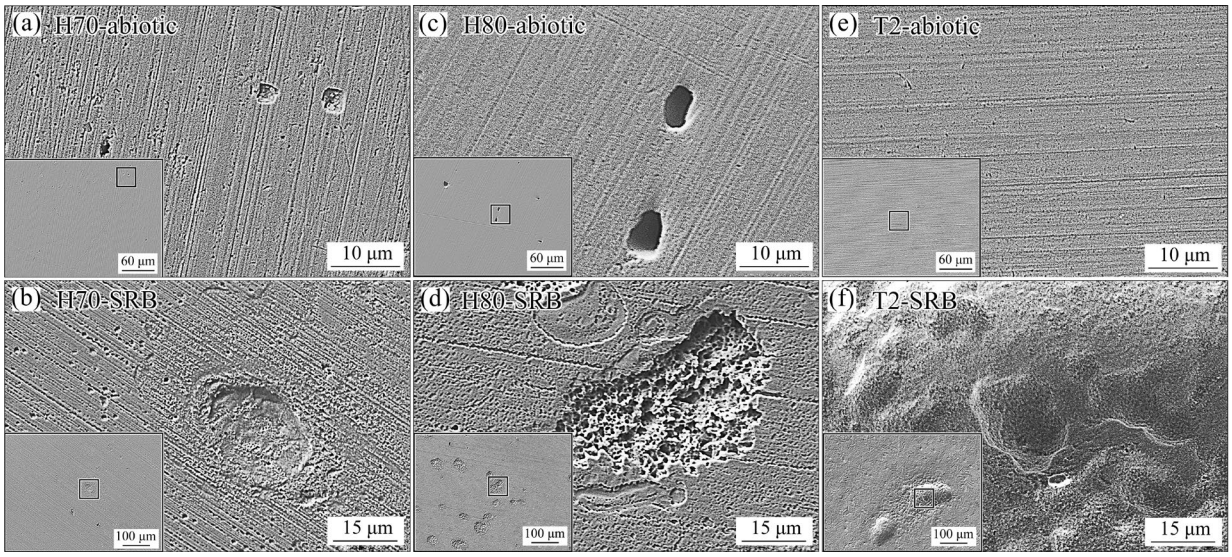

Fig. 7 Corrosion morphology of brass and copper after 336 h of immersion in sterile (a, c, e) and inoculated (b, d, f) media: (a, b) H70; (c, d) H80; (e, f) T2

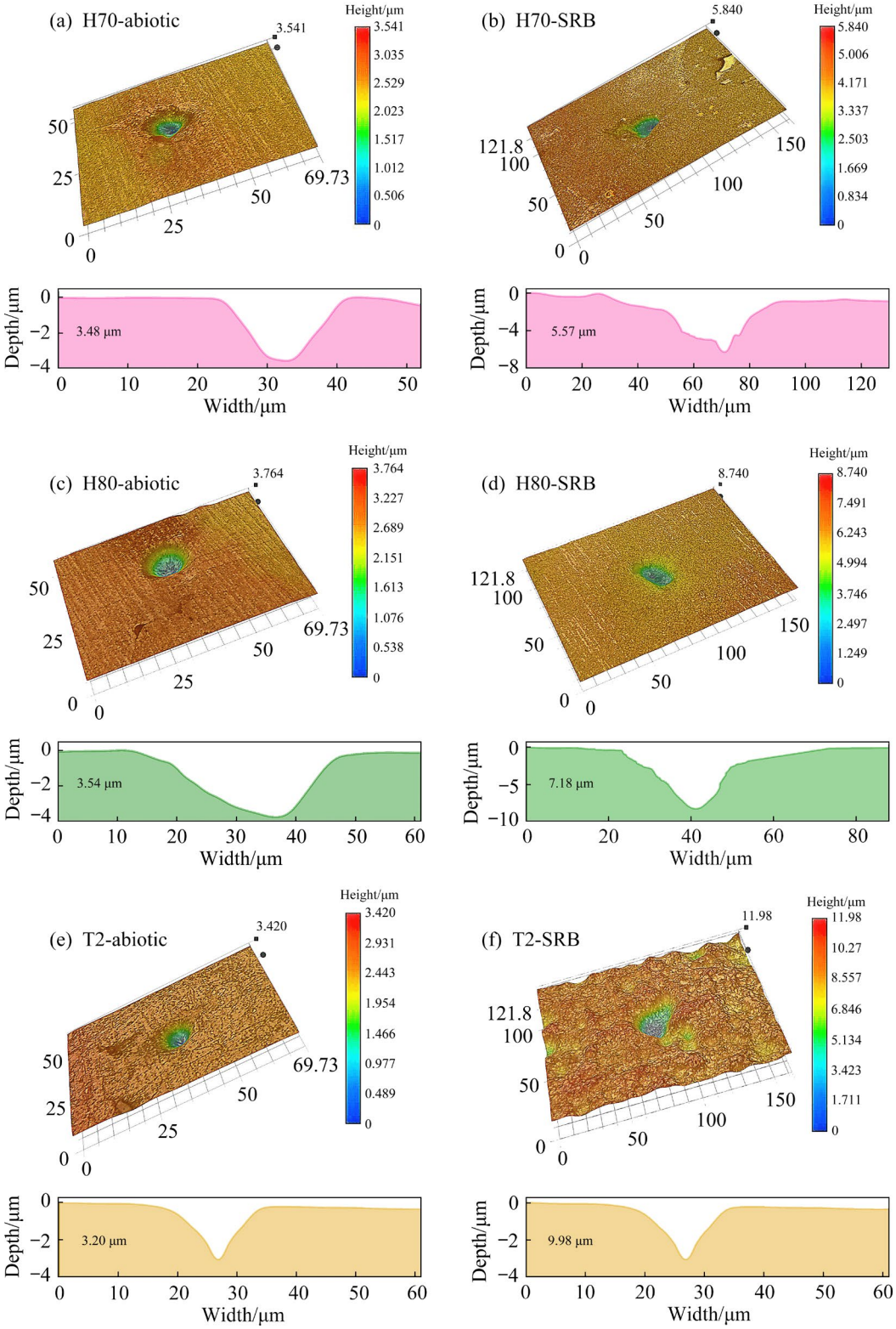

Fig. 8 3D morphology of surfaces of brass and copper after 336 h of immersion in sterile (a, c, e) and inoculated (b, d, f) media: (a, b) H70; (c, d) H80; (e, f) T2

brass and T2 copper were 5.57, 7.18 and 9.98 μm, respectively. Obviously, the maximum depth of the corrosion pit increased with the increase of Cu content in the sample matrix. Figure 9 presents the pit depths and average depth of 10 random corrosion pits on each sample surfaces in the sterile and inoculated media. The evolution of the pit depths was identical to that in Fig. 8.

D. desulfuricans cells accelerated the local corrosion of H70 brass, H80 brass and T2 copper, and the accelerating effect was intensified with the increase of Cu content in the sample matrix.

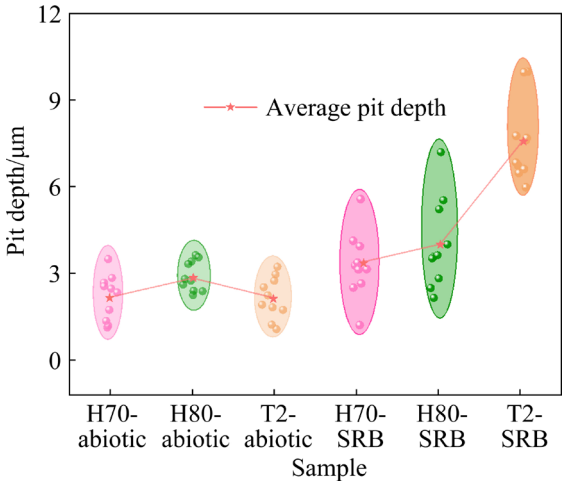

Fig. 9 Depth of 10 random pits on surfaces of brass and copper after 336 h of immersion in sterile and inoculated media

3.5 Polarization curves

The potentiodynamic polarization curves of the H70 brass, H80 brass and T2 copper in the sterile and inoculated media are presented in Figs. 10(a, b). In the sterile medium, little difference was observed from the polarization curves of the three types of copper alloys. The anode branches of these polarization curves showed a typical characteristic of anodic dissolution, while high Tafel slope and certain diffusion control were the distinctive feature for the cathode branches. In comparison of the sterile medium, all of the polarization curves for the three samples in the inoculated medium with *D. desulfuricans* moved to the right-down direction, reflecting the acceleration of the anodic dissolution as well as cathodic reduction. The acceleration degree for T2 copper was much remarkable. The cathode branches of the polarization curves for the H70 brass and H80 brass showed a typical characteristic of the cathodic reduction control without the diffusion effect. But

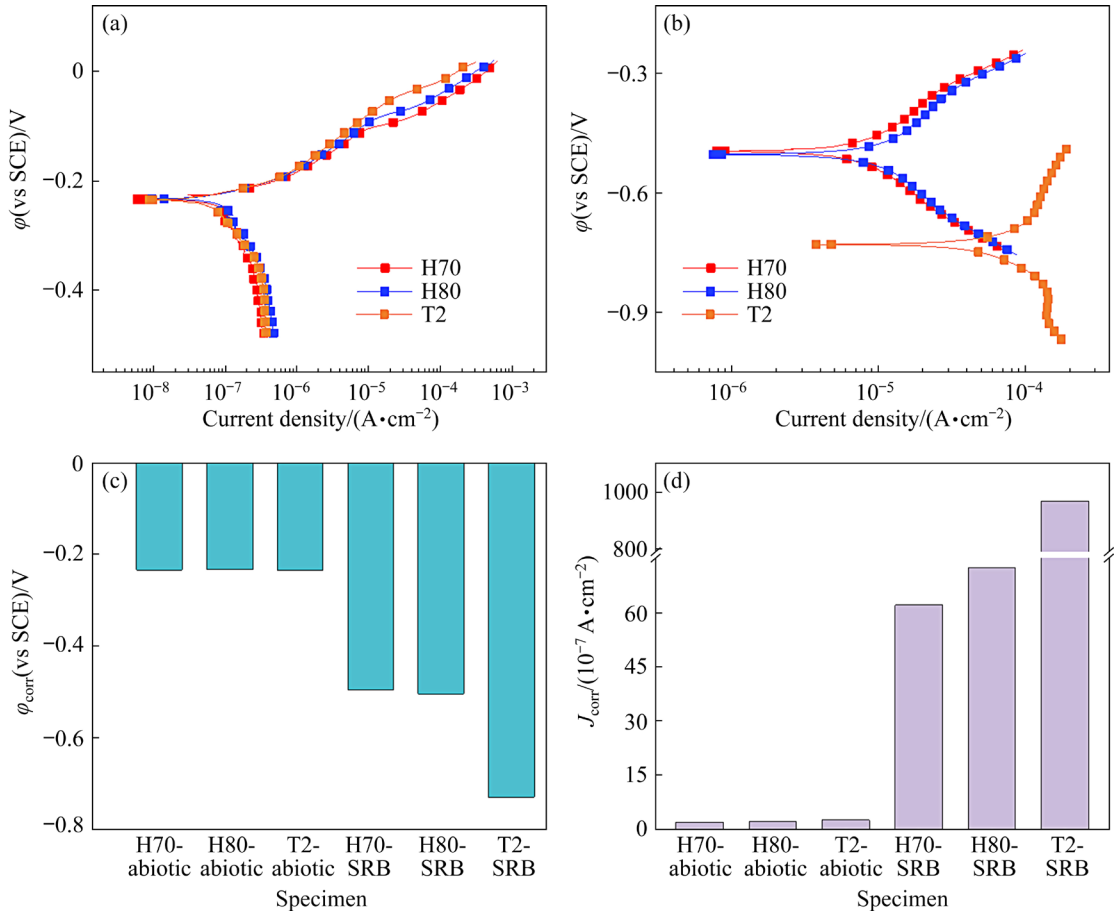

Fig. 10 Polarization curves of brass and copper after 336 h of immersion in sterile (a) and inoculated (b) media, and corrosion potential φ_{corr} (c) and corrosion current density J_{corr} (d) of brass and copper after 336 h of immersion in sterile and inoculated media

obvious diffusion control featured the cathode branches of the polarization curve for T2 copper in this environment, and the limited diffusion current density was about 1.5×10^{-4}A/cm^2.

The polarization curves were fitted using the Tafel equations [33]:

$$\eta_a=\varphi-\varphi_{corr}=-b_a\lg(|J_{corr}|)+b_a\lg(|J|) \quad (2)$$

$$\eta_c=\varphi_{corr}-\varphi=-b_c\lg(|J_{corr}|)+b_c\lg(|J|) \quad (3)$$

where η_a and η_c represent the overpotentials of the anodic and cathodic electrodes, φ and φ_{corr} represent the electrode potential and the corrosion potential, b_a and b_c represent the anode and cathode slopes, and J_{corr} represents the corrosion current density. The fitting results are presented in Table 1. The corrosion rate of the T2 copper in the inoculated medium was mainly controlled by the diffusion, thus the cathode slope b_c tended to the infinite. As shown in Figs. 10(c, d), after 336 h of immersion in the sterile environment, J_{corr} and φ_{corr} values of the H70 brass, H80 brass and T2 copper were all distributed in the ranges of $(1.9-2.5)\times10^{-7}$A/cm^2 and −0.233 to 0.235 V (vs SCE). Obviously, the differences in J_{corr} and φ_{corr} values for the three samples were small, which was consistent with the results of the corrosion rate (Fig. 3). φ_{corr} of the three types of copper alloys significantly shifted to the negative direction in the inoculated medium, showing the accelerated rate of cathode reaction [34]. J_{corr} of the H70 brass, H80 brass and T2 copper increased to 6.21×10^{-6}, 7.25×10^{-6} and 9.73×10^{-5} A/cm^2, respectively (Figs. 10(c, d)). The facts demonstrated that the metabolism of the *D. desulfuricans* cells greatly increased the corrosion rate of the three types of copper alloys.

3.6 EIS result and analysis

Figures 11 and 12 show the EIS evolution of the three types of copper alloys over time in the sterile and inoculated media, respectively. In sterile medium, the Nyquist plots of all samples showed a characteristic of single and compressive capacitive arc. The radius of the capacitive arc gradually increased with time, showing the gradually decreasing corrosion rate. The accumulation of the corrosion products on the sample surface was responsible for this phenomenon. During the whole experiment, the impedance value of the T2 copper in the sterile medium was slightly higher than that of H70 brass and H80 brass. The equivalent circuit in Fig. 11(a) was used to fit the EIS data of the samples in the sterile medium. In this equivalent circuit, R_s was the solution resistance, and R_f and Q_f were the resistance and capacitance of the corrosion products, R_{ct} and Q_{dl} were the charge transfer resistance and double layer capacitance, respectively. A constant phase element (CPE) was used to simulate the corrosion products and double layer capacitors. The impedance (Z_{CPE}) of the CPE was as follows:

$$Z_{CPE}=Y_0^{-1}(j\omega)^{-n} \quad (4)$$

where ω is the angular frequency (rad/s), j is the imaginary number, $j=(-1)^{1/2}$, and Y_0 and n are the two parameters of the CPE, respectively.

Table 2 shows the EIS fitting results of the H70 brass, H80 brass and T2 copper in the sterile medium, and the evolution of $R_{ct}+R_f$ values over time is shown in Fig. 13(a). $R_{ct}+R_f$ values of the three types of copper alloys were very large, and slightly increased with time. The facts indicate that the H70 brass, H80 brass and T2 copper all have good corrosion resistance during the whole experiment period in this environment. Particularly, the evolution plots of $R_{ct}+R_f$ values for T2 copper was slightly higher than those of H70 brass and H80 brass, corresponding to the results of the corrosion rate.

Table 1 Fitting results of polarization curves of brass and copper after 336 h of immersion in sterile and inoculated media

Specimen	φ_{corr} (vs SCE)/V	J_{corr}/(A·cm^{-2})	b_c/(V·dec^{-1})	b_a/(V·dec^{-1})
H70-abiotic	−0.234	1.93×10^{-7}	−0.959	0.069
H80-abiotic	−0.233	2.23×10^{-7}	−0.740	0.080
T2-abiotic	−0.235	2.54×10^{-7}	−1.520	0.097
H70-SRB	−0.495	6.21×10^{-6}	−0.238	0.202
H80-SRB	−0.504	7.25×10^{-6}	−0.235	0.170
T2-SRB-336h	−0.729	9.73×10^{-5}	−	0.777

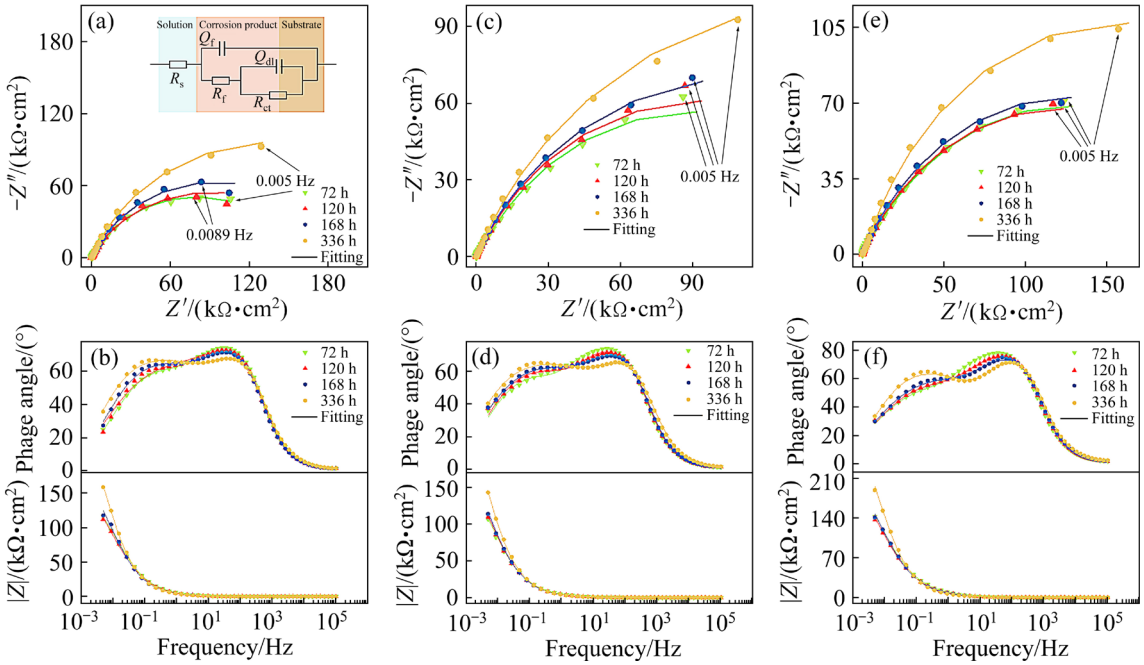

Fig. 11 Nyquist (a, c, e) and Bode (b, d, f) plots of brass and copper in sterile medium: (a, b) H70; (c, d) H80; (e, f) T2

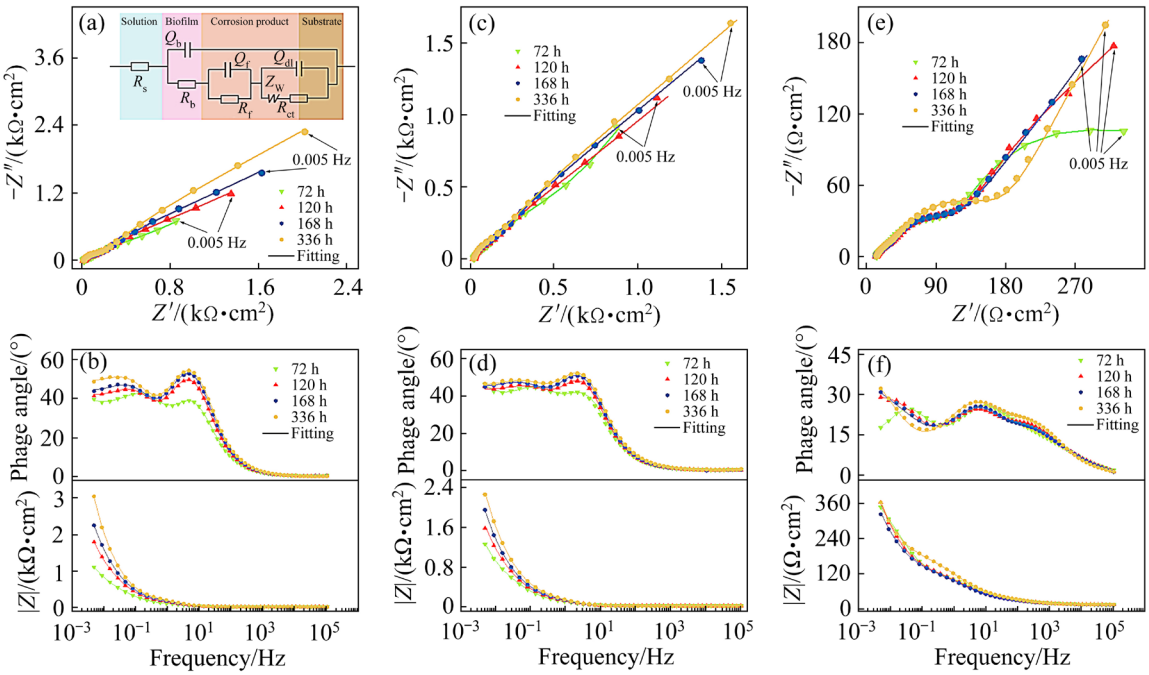

Fig. 12 Nyquist (a, c, e) and Bode (b, d, f) plots of brass and copper in inoculated medium: (a, b) H70; (c, d) H80; (e, f) T2

Compared with that in the sterile medium, the radius of the capacitance arc in the Nyquist plot for all samples was greatly reduced in the inoculated medium, showing the much higher corrosion rate of the samples in this environment. Besides, the phase response of the samples in the inoculated medium moved to the low frequency region, which was relative to the lower protective effect of the biofilm or corrosion products film on the sample surface. Therefore, the redox reaction at the sample/solution interface may be simultaneously affected by electrode potential, biofilm and diffusion process. EIS results of the samples in the inoculated medium could be fitted using the equivalent circuit in Fig. 12(a). In this equivalent circuit, R_b and Q_b respectively represent the resistance and capacitance of the biofilm, and Z_W represents the Warburg impedance.

Table 2 EIS fitting results of brass and copper in sterile medium

Specimen	R_s/(Ω·cm^2)	Y_f/(10^{-5} S·s^n·cm^{-2})	n_f	R_f/(Ω·cm^2)	Y_{dl}/(10^{-5} S·s^n·cm^{-2})	n_{dl}	R_{ct}/(kΩ·cm^2)
H70-72h	27.26	2.12	0.91	5377	3.27	0.66	156.7
H70-120h	26.88	2.38	0.90	3026	3.18	0.60	186.4
H70-168h	25.98	2.64	0.89	3014	3.46	0.68	189.6
H70-336h	26.01	2.65	0.87	2121	3.20	0.71	280.5
H80-72h	25.76	2.82	0.89	7560	4.68	0.67	175.7
H80-120h	25.64	2.86	0.88	4540	4.46	0.67	186.8
H80-168h	25.44	2.77	0.88	2394	4.30	0.65	228.5
H80-336h	24.95	2.60	0.86	1499	3.93	0.68	311.3
T2-72h	27.05	1.36	0.92	10630	2.97	0.60	244.8
T2-120h	26.83	1.30	0.92	5444	3.01	0.60	243.5
T2-168h	27.15	1.25	0.91	3297	2.99	0.62	256.2
T2-336h	26.75	1.19	0.90	2640	3.12	0.72	318.5

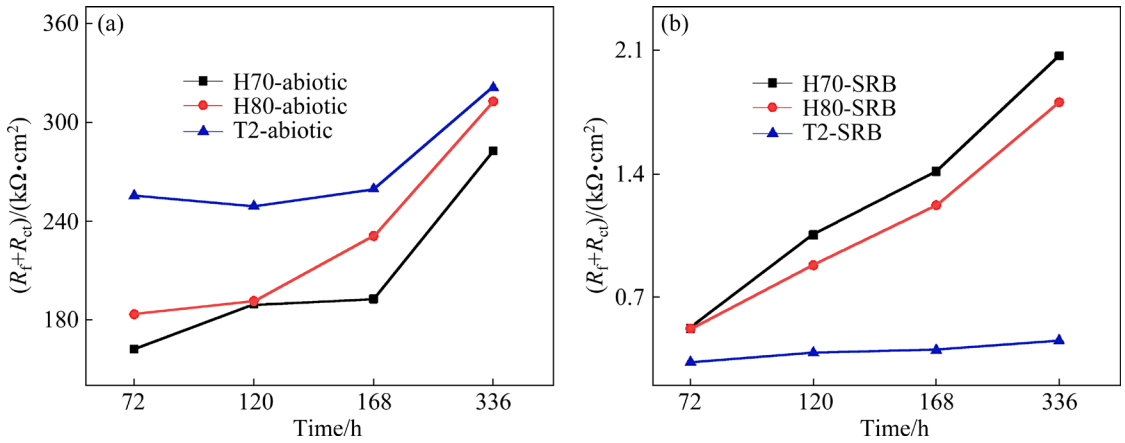

Fig. 13 R_f+R_{ct} values of brass and copper in sterile (a) and inoculated (b) media

The fitting results are shown in Table 3, where W is the impedance value of Z_W. The evolution of R_{ct}+R_f values with time is presented in Fig. 13(b). In the whole experiment, R_{ct}+R_f values of the three types of copper alloys increased gradually with the time. With the increase of Cu content in the sample matrix, R_{ct}+R_f value of the sample successively decreased, showing the gradually intensified corrosion process. From Tables 2 and 3, R_{ct}+R_f values of the three copper alloys were distributed in the range of 150−320 kΩ·cm^2 in the sterile environment, while these in the inoculated environment were reduced to 0.2−2.1 kΩ·cm^2. The latter was about one in a thousand of the former, showing that the metabolism of the *D. desulfuricans* cells sharply increased the corrosion rate of the three types of copper alloys.

4 Discussion

4.1 SRB corrosion of copper alloys

In the sterile environment, the corrosion products on the surfaces of the three types of copper alloys are relatively thin and mainly the oxides, such as Cu_2O, CuO and ZnO [35] (Figs. 4 and 5). In the inoculated environment with *D. desulfuricans*, all surfaces of the copper alloys are covered by a thick mixture of the oxides and sulfur-containing compounds, such as Cu_2S, ZnS and $CuSO_4$ (Figs. 4 and 5). The sulfur-containing compounds are related to the metabolism of *D. desulfuricans*. During the metabolism of *D. desulfuricans*, organic carbon source, such as lactate, acts as the electron donor and sulfate as electron acceptor [36]:

Table 3 EIS fitting results of brass and copper in inoculated medium

Specimen	R_s/ ($\Omega\cdot cm^2$)	Y_b/(10^{-4} $S\cdot s^n\cdot cm^{-2}$)	n_b	R_b/ ($\Omega\cdot cm^2$)	Y_f/(10^{-4} $S\cdot s^n\cdot cm^{-2}$)	n_f	R_f/ ($\Omega\cdot cm^2$)	Y_{dl}/(10^{-3} $S\cdot s^n\cdot cm^{-2}$)	n_{dl}	R_{ct}/ ($\Omega\cdot cm^2$)	W/ ($S\cdot s^{0.5}$)
H70-72h	19.7	7.47	0.84	4.69	4.11	0.89	82.72	3.94	0.83	441.8	0.00582
H70-120h	18.79	5.71	0.88	8.13	2.78	0.90	170.8	3.65	0.83	883.5	0.00334
H70-168h	17.87	5.19	0.89	8.30	2.51	0.90	207.4	3.29	0.83	1207	0.00243
H70-336h	17.67	4.64	0.89	12.50	2.55	0.89	232.2	2.82	0.82	1837	0.00148
H80-72h	22.49	8.03	0.87	6.50	8.79	0.88	83.05	3.69	0.81	440.5	0.00422
H80-120h	21.25	9.22	0.87	8.73	5.56	0.89	156.1	3.73	0.81	726.2	0.00330
H80-168h	20.42	8.63	0.88	9.20	5.54	0.87	194.4	3.74	0.82	1029	0.00266
H80-336h	20.47	8.21	0.87	10.92	5.06	0.89	196.6	2.88	0.75	1611	0.00200
T2-72h	13.08	9.66	0.55	27.95	9.45	0.70	85.6	20.2	0.79	247.2	0.09563
T2-120h	12.86	5.69	0.61	26.40	20.1	0.62	87.31	23.0	0.76	298.5	0.02867
T2-168h	12.53	6.15	0.61	22.88	20.5	0.61	97.47	29.2	0.72	219.8	0.01990
T2-336h	13.12	4.37	0.65	29.49	17.9	0.60	145.4	14.3	0.76	310.2	0.01256

$$CH_3CHOHCOO^-+H_2O\rightarrow CH_3COO^-+CO_2+4H^++4e \quad (5)$$

$$SO_4^{2-}+9H^++8e\rightarrow HS^-+4H_2O \quad (6)$$

HS^- formed from the sulfate reduction is the main sulfide in the inoculated environment. H_2S could be generated in the medium via the combination of HS^- and H^+, and then the saturated H_2S in the medium could escape to the gas phase in the top of the bottles. At the end of the experiment, the production of H_2S decreased as the number of *D. desulfuricans* cells decreased. Thus, it allowed the H_2S gas at the top of the bottles to dissolve into the medium to form HS^- and H^+, maintaining a dynamic HS^- equilibrium between the gas and liquid phases throughout the experiment [23]:

$$HS^-+H^+\rightleftharpoons H_2S \quad (7)$$

Therefore, there is always a high concentration of HS^- existing in this medium. In aqueous electrolyte, the element copper could react with HS^- to form Cu_2S [22,36]:

$$2Cu+HS^-+H^+\rightarrow Cu_2S+H_2(g) \quad (8)$$

The combination of the above chemical, electrochemical and bio-electrochemical processes would lead to the serious copper corrosion, which is the so-called MIC caused by metabolites, abbreviated as M-MIC [23,37]. The EDS and XPS results (Figs. 5 and 6) of the corrosion products could confirm the corrosion process of the copper and its alloys.

The dense Cu_2O film producing in the sterile environment is a good protective barrier, preventing the metal matrix from further corrosion [38,39]. However, in the inoculated medium, the dense Cu_2O film on the metal surface is partially replaced by the Cu_2S film, and the protective effect of the film accordingly decreases, leading to the increasing corrosion rate of the metal matrix [6,40,41]. In addition, a large number of sulfides (such as H_2S, and HS^-) could generate under the metabolism of *D. desulfuricans* cells, which could locally vulcanize the film layer on the sample surface. It is easier for anions to penetrate the film layer and then accumulate at the metal/layer interface, resulting in the accelerated metal corrosion [42]. Therefore, the biocatalysis of the *D. desulfuricans* cells is another reason for the MIC of the copper and its alloys.

4.2 Effect of microstructure and Zn content on SRB corrosion of copper alloys

The metal microstructure could alter the electrochemical activity of the metal, affecting its corrosion sensitivity [43,44]. RALSTON and BIRBILIS [45] pointed out that the grain refinement could increase the corrosion sensitivity of metals. Actually, the grain refinement could result in a large number of defects in the metal matrix and reactive sites on the metal surface, which could increase the electrochemical activity of the metal surface. Besides, the microstructure could

affect the microorganism attachment on the metal surface, and then the MIC process. Bacterial attachment firstly occurs on or near grain boundaries. The attachment degree on the metal surface with fine grains is higher than that with coarse grains, and there is a negative correlation between bacterial attachment degree and grain size [46,47]. As shown in Fig. 1, (Cu, Zn) phases dominate the microstructure of H70 brass and H80 brass, while the polygonal grains with obvious grain boundaries is the main microstructure for T2 copper. Therefore, one can reasonably conclude that the clear grain boundary in the T2 copper is beneficial for the attachment of the *D. desulfuricans* cells, and hence the MIC on the metal surface. In addition, the bacterial attachment process is related to the surface potential [48]. The clear grain boundary on the surface of T2 copper sample provides a suitable local-potential for the attachment of the *D. desulfuricans* cells in a certain area.

The composition of the alloy matrix could alter the MIC process via two ways. Firstly, as shown in Fig. 1, the zinc-rich phase in the H70 and H80 brasses is easy to dissolve in an aqueous electrolyte, promoting the generation of the zinc oxide on the metal surface, which could prevent the cell attachment [49]:

$$Zn \rightarrow Zn^{2+}+2e \quad (9)$$

$$Zn^{2+}+H_2O \rightarrow ZnO+2H^{+} \quad (10)$$

Therefore, the amount of the sessile cells on the surfaces of the H70 and H80 brasses is much less than that on the T2 copper surface (Fig. 2). As a matter of course, the corrosion rate of the T2 copper is much higher than that of the H70 and H80 brasses under the action of the *D. desulfuricans* cells. Secondly, it is reported that a certain concentration of the copper ions (Cu^{+} and Cu^{2+}) is toxic to the microorganism, which could reduce the metabolism of the *D. desulfuricans* cells [50]. However, as shown in the Reaction (8), the sulfides from the metabolism of the *D. desulfuricans* cells combine with the cuprous ions to form extremely insoluble Cu_2S, which resists the toxicity of the cuprous ions [15,23,51]. As shown in Fig. 5, the content of element S in the corrosion products surface increased with the increase of the copper content in the sample matrix. From this perspective, a higher degree of attachment on the metal surface could be one of the survival strategies for the *D. desulfuricans* cells. Therefore, with the increase of Cu content in the metal matrix, the concentration of the *D. desulfuricans* cells on the metal surface and hence the corresponding corrosion rate of the metal are increasing.

5 Conclusions

(1) In the sterile environment, the corrosion rates of the three types of copper alloys are in the range of 2−3 μm/a, showing the low corrosion rate and high corrosion resistance in this environment. However, in the inoculated environment with *D. desulfuricans* cells, the corrosion rates of H70 brass, H80 brass and T2 copper are 5.1, 6.8 and 249 μm/a, respectively. The corrosion rates of the three types of copper alloys significantly increase in this environment, especially the T2 copper.

(2) In the sterile environment, general corrosion is the main corrosion style of the three types of copper alloys and the corrosion products on their surfaces are mainly composed of metal oxides, such as Cu_2O, CuO and ZnO. In the inoculated environment, obvious pitting corrosion takes place on the surfaces of the H70 brass and H80 brass, while general corrosion and pitting corrosion simultaneously dominate the corrosion process of the T2 copper. An additional mixture of Cu_2S, ZnS and $CuSO_4$ exists in the corrosion products in this environment, and the content of element S in the corrosion products increases with the increase of the copper content in the sample matrix.

(3) $R_{ct}+R_f$ values of the three types of copper alloys are in the range of 150−320 $k\Omega \cdot cm^2$ in the sterile environment, while these in the inoculated environment are reduced to 0.2−2.1 $k\Omega \cdot cm^2$. The metabolism of the *D. desulfuricans* cells sharply accelerates the corrosion process of three types of copper alloys, especially the T2 copper. The negative shift of the corrosion potential and the sharp enhancement of the corrosion current density confirm the pronounced MIC of the alloys.

CRediT authorship contribution statement

Shu-hua XU: Investigation, Writing − Original draft; **Qin WANG:** Methodology; **Zhuo-wei TAN:** Visualization; **Xiao-bao ZHOU:** Methodology; **Cong LI** and **Zhen-sheng WANG:** Verification, Resources; **Tang-**

qing WU: Conceptualization, Writing − Review & editing, Supervision, Funding acquisition.

Declaration of competing interest

The authors declare that they have no known competing financial interests or personal relationships that could have appeared to influence the work reported in this paper.

Data availability

The raw/processed data will be made available on request.

Acknowledgments

We are grateful for the financial support of the National Natural Science Foundation of China (No. 51971191), Scientific Research Project of Education Department of Hunan Province (Nos. 22B0178, 22C0075), Hunan Provincial Innovation Foundation for Postgraduate (No. CX20220558), and the National Scholarship Foundation (No. 202008430013).

References

[1] LI Xiao-gang, ZHANG D, LIU Z, LI Z, DU C, DONG C. Materials science: Share corrosion data [J]. Nature, 2015, 527: 441−442.

[2] HOU Bao-rong, LI Xiao-gang, MA Xiu-min, DU Cui-wei, ZHANG Da-wei, ZHENG Meng, XU Wei-chen, LU Dong-zhu, MA Fu-bin. The cost of corrosion in China [J]. NPJ Materials Degradation, 2017, 1: 1−4.

[3] FATAH M C, ISMAIL M C, WAHJOEDI B A. Effects of sulphide ion on corrosion behaviour of X52 steel in simulated solution containing metabolic products species: A study pertaining to microbiologically influenced corrosion (MIC) [J]. Corrosion Engineering Science and Technology, 2013, 48: 211−220.

[4] LIU W. Rapid MIC attack on 2205 duplex stainless steel pipe in a yacht [J]. Engineering Failure Analysis, 2014, 42: 109−120.

[5] GUO Na, MAO Xiao-min, HUI Xin-rui, GUO Zhang-wei, LIU Tao. Corrosion behavior of 316L stainless steel in media containing pyomelanin secreted by *pseudoalteromonas lipolytica* [J]. Journal of Chinese Society for Corrosion and Protection, 2022, 42: 743−751.

[6] LIU Hai-xian, HE Jia-qi, JIN Zheng-yu, LIU Hong-wei. Pitting corrosion behavior and mechanism of 316L stainless steel induced by marine fungal extracellular polymeric substances [J]. Corrosion Science, 2023, 224: 111485.

[7] GU Ting-yue, JIA Ru, UNSAL T, XU Da-ke. Toward a better understanding of microbiologically influenced corrosion caused by sulfate reducing bacteria [J]. Journal of Materials Science & Technology, 2019, 35: 631−636.

[8] DOU Wen-wen, XU Da-ke, GU Ting-yue. Biocorrosion caused by microbial biofilms is ubiquitous around us [J]. Microbial Biotechnology, 2021, 14: 803−805.

[9] ZHOU Xiao-bao, WANG Qin, SU Hui, WANG Xuan-kai, WU Tang-qing, ZHANG Ming-hua, LI Zhi, YIN Fu-cheng. Accelerated tidal corrosion of X80 pipeline steel by *Desulfovibrio desulfuricans* [J]. Corrosion Science, 2022, 201: 110272.

[10] GAO Qiu-ying, ZENG Wen-guang, WANG Heng, LIU Yuan-cong, HU Jun-ying. Effect of fluid scouring on sulfate reducing bacteria induced corrosion of pipeline steel [J]. Journal of Chinese Society for Corrosion and Protection, 2023, 43: 1087−1093.

[11] ZHOU Xiao-bao, ZHOU Zhao-fen, WU Tang-qing, LI Cong, LI Zhi. Effects of non-viable microbial film on corrosion of pipeline steel in soil environment [J]. Corrosion Communications, 2021, 3: 23−33.

[12] KING R A, MILLER J D A. Corrosion by the sulphate-reducing bacteria [J]. Nature, 1971, 233: 491−492.

[13] LEE W, LEWANDOWSKI Z, NIELSEN P H, HAMILTON W A. Role of sulfate-reducing bacteria in corrosion of mild steel: A review [J]. Biofouling, 1995, 8: 165−194.

[14] LV Mei-ying, DU Min. A review: Microbiologically influenced corrosion and the effect of cathodic polarization on typical bacteria [J]. Reviews in Environmental Science and Bio/Technology, 2018, 17: 431−446.

[15] GUO Na, MAO Xiao-min, LIU Tao, HUI Xin-rui, GUO Zhang-wei, TAN Bo-wen, SHAO Kai-yuan, LI Xiao Feng, ZENG Zhen-shun. Corrosion mechanism of copper in seawater containing the bacterial pyomelanin with redox activity [J]. Corrosion Science, 2022, 204: 110407.

[16] XU Da-ke, GU Ting-yue. Carbon source starvation triggered more aggressive corrosion against carbon steel by the *Desulfovibrio vulgaris* biofilm [J]. International Biodeterioration & Biodegradation, 2014, 91: 74−81.

[17] LIU Hong-wei, CHEN Cui-ying, ASIF M, ZHAO Tong, LEI Bing, MENG Guo-zhe, LIU Hong-fang. Mechanistic investigations of corrosion and localized corrosion of X80 steel in seawater comprising sulfate-reducing bacteria under continuous carbon starvation [J]. Corrosion Communications, 2022, 8: 70−80.

[18] WANG Di, YANG Chun-tian, SALEH M A, ALOTAIBI M D, MOHAMED M E, XU Da-ke, GU Ting-yue. Conductive magnetite nanoparticles considerably accelerated carbon steel corrosion by electroactive *Desulfovibrio vulgaris* biofilm [J]. Corrosion Science, 2022, 205: 110440.

[19] WANG Xuan-kai, XIE Yi, FENG Chao, DING Zhi-min, LI Deng-ke, ZHOU Xiao-bao, WU Tang-qing. Atmospheric corrosion of tin coatings on H62 brass and T2 copper in an urban environment [J]. Engineering Failure Analysis, 2022, 141: 106735.

[20] LU Xiao, LIU Yu-wei, ZHAO Hong-tao, PAN Chen, WANG Zhen-yao. Corrosion behavior of copper in extremely harsh marine atmosphere in Nansha Islands, China [J]. Transactions of Nonferrous Metals Society of China, 2021, 31: 703−714.

[21] SONG Qi-ning, LI Hui-lin, ZHANG Hao-nan, HONG Hao, XU Nan, ZHANG Gen-yuan, BAO Ye-feng, QIAO Yan-xin. Correlation between microstructure and corrosion and cavitation erosion behaviors of nickel aluminum bronze [J]. Transactions of Nonferrous Metals Society of China, 2022,

32: 2948−2964.

[22] HUTTUNEN S E, RAJALA P, CARPÉN L. Corrosion behaviour of copper under biotic and abiotic conditions in anoxic ground water: Electrochemical study [J]. Electrochimica Acta, 2016, 203: 350−365.

[23] DOU Wen-wen, JIA Ru, JIN Peng, LIU Jia-lin, CHEN Shou-gang, GU Ting-yue. Investigation of the mechanism and characteristics of copper corrosion by sulfate reducing bacteria [J]. Corrosion Science, 2018, 144: 237−248.

[24] DOU Wen-wen, LIU Jia-lin, CAI Wei-zhen, WANG Di, JIA Ru, CHEN Shou-gang, GU Ting-yue. Electrochemical investigation of increased carbon steel corrosion via extracellular electron transfer by a sulfate reducing bacterium under carbon source starvation [J]. Corrosion Science, 2019, 150: 258−267.

[25] BASTOS M C, MENDONÇA M H, NETO M M M, ROCHA M M G S, PROENÇA L, FONSECA I T E. Corrosion of brass in natural and artificial seawater under anaerobic conditions [J]. Journal of Applied Electrochemistry, 2008, 38: 627−635.

[26] ZHAO Xiao-dong, YAN Chao-ming, SHAO Jing, YANG Jie, LIU Jie, SUN Dong-yu, WANG Shuai. Influence of *Pseudomonas aeruginosa* and Sulfate-reducing bacteria composite on the corrosion behavior of brass [J]. International Journal of Electrochemical Science, 2019, 14: 6468−6477.

[27] VAROL T, GÜLER O, AKÇAY S B, AKSA H C. The effect of silver coated copper particle content on the properties of novel Cu−Ag alloys prepared by hot pressing method [J]. Powder Technology, 2021, 384: 236−246.

[28] WANG Qin, ZHOU Xiao-bao, MA Qiao, WU Tang-qing, LIU Meng, ZHANG Ming-hua, LI Zhi, YIN Fu-cheng. Selected corrosion of X80 pipeline steel welded joints induced by *Desulfovibrio desulfuricans* [J]. Corrosion Science, 2022, 202: 110313.

[29] PAN Chen, LV Wang-yan, WANG Zhen-yao, SU Wei, WANG Chu-an, LIU Shi-nian. Atmospheric corrosion of copper exposed in a simulated coastal-industrial atmosphere [J]. Journal of Materials Science & Technology, 2017, 33: 587−595.

[30] LU Xiao, LIU Yu-wei, LIU Miao-ran, WANG Zhen-yao. Corrosion behavior of copper T2 and brass H62 in simulated Nansha marine atmosphere [J]. Journal of Materials Science & Technology, 2019, 35: 1831−1839.

[31] WANG Xuan-Kai, SU Hui, XIE Yi, WANG Jun, FENG Chao, LI Deng-ke, WU Tang-qing. Atmospheric corrosion of T2 copper and H62 brass exposed in an urban environment [J]. Materials Chemistry and Physics, 2023, 299: 127487.

[32] PU Ya-nan, DOU Wen-wen, CHENG Y F, CHEN Shou-gang, XU Zi-xuan, CHEN Zhao-yang. Biogenic H2S and extracellular electron transfer resulted in two-coexisting mechanisms in 90/10Cu−Ni alloy corrosion by a sulfate-reducing bacteria [J]. Corrosion Science, 2023, 211: 110911.

[33] CAO chu-nan. Principles of electrochemistry of corrosion [M]. Beijing: Chemical Industry Press, 2008. (in Chinese)

[34] YANG Yang, SU Hui, LIU Lan-lan, XU Song, ZHONG Zhen, ZHOU Xiao-bao, WU Tang-qing. Inhibition roles of molybdate and borate on Q235 steel corrosion in resistance reducing agent [J]. Journal of Iron and Steel Research International, 2023, 30: 1477−1489.

[35] WANG Yong-xia, XIANG Hong-liang, YANG Cai-ping, LIU Dong. Corrosion resistance of copper-bearing duplex stainless steel in culture medium without and with bacteria [J]. Journal of Chinese Society for Corrosion and Protection, 2014, 34: 558−565.

[36] PU Ya-nan, CHENG Y F, DOU Wen-wen, XU Zi-xuan, HOU Su, HOU Yue, CHEN Shou-gang. Microbiologically influenced corrosion behavior of 70/30 Cu−Ni alloy exposed to carbon starvation environments with different aggressiveness: Pitting mechanism induced by *Desulfovibrio vulgaris* [J]. Corrosion Science, 2023, 222: 111427.

[37] LIU Hai-xian, JIN Zheng-yu, WANG Zhi, LIU Hong-fang, MENG Guo-zhe, LIU Hong-wei. Corrosion inhibition of deposit-covered X80 pipeline steel in seawater containing *Pseudomonas stutzeri* [J]. Bioelectrochemistry, 2023, 149: 108279.

[38] MA A L, JIANG S L, ZHENG Y G, KE W. Corrosion product film formed on the 90/10 copper–nickel tube in natural seawater: Composition/structure and formation mechanism [J]. Corrosion Science, 2015, 91: 245−261.

[39] LIAO Wen-pei, LIU Hai-xian, JIN Zheng-yu, WANG Zhi, LIU Hong-wei. Synergistic inhibition effect of ultraviolet irradiation and benzalkonium chloride on the corrosion of 316L stainless steel caused by *Aspergillus terreus* [J]. Bioelectrochemistry, 2023, 153: 108485.

[40] CHEN J, QIN Z, WU L, NOËL J J, SHOESMITH D W. The influence of sulphide transport on the growth and properties of copper sulphide films on copper [J]. Corrosion Science, 2014, 87: 233−238.

[41] LIU Hai-xian, ZHANG Wan-qing, ZHAO Zi-long, LAI Huan-sheng, LIU Hong-wei. Broken passive film and subsequent pitting corrosion behavior of 2205 duplex stainless steel induced by marine fungus *Aspergillus terreus* in artificial seawater [J]. Corrosion Science, 2023, 218: 111147.

[42] KONG De-cheng, XU Ao-ni, DONG Chao-fang, MAO Fei-xiong, XIAO Kui, LI Xiao-gang, MACDONALD D D. Electrochemical investigation and ab initio computation of passive film properties on copper in anaerobic sulphide solutions [J]. Corrosion Science, 2017, 116: 34−43.

[43] ZHANG Da-lei, LIU Ran, LIU Ying-shuang, XING Shao-hua, HE Zong-hao, QIAN Yao, LIU Jin-zeng, DOU Xiao-hui, ZHANG Xin-wei. Combined experimental and simulation study on corrosion behavior of B10 copper–nickel alloy welded joint under local turbulence [J]. Journal of Iron and Steel Research International, 2023, 30: 1598−1612.

[44] ZHANG Meng-han, LIU Sheng-dan, JIANG Jing-yu, WEI Wei-chang. Effect of Cu content on intergranular corrosion and exfoliation corrosion susceptibility of Al−Zn−Mg−(Cu) alloys [J]. Transactions of Nonferrous Metals Society of China, 2023, 33: 1963−1976.

[45] RALSTON K D, BIRBILIS N. Effect of grain size on corrosion: A review [J]. Corrosion, 2010, 66: 7500501−7500513.

[46] SREEKUMARI K R, NANDAKUMAR K, KIKUCHI Y. Bacterial attachment to stainless steel welds: Significance of substratum microstructure [J]. Biofouling, 2001, 17: 303−316.

[47] JAVED M A, STODDART P R, MCARTHUR S L, WADE S A. The effect of metal microstructure on the initial attachment of *Escherichia coli* to 1010 carbon steel [J]. Biofouling, 2013, 29: 939−952.
[48] LIU Tao, CHENG Y F. The influence of cathodic protection potential on the biofilm formation and corrosion behaviour of an X70 steel pipeline in sulfate reducing bacteria media [J]. Journal of Alloys and Compounds, 2017, 729: 180−188.
[49] CHEN B Y, UTGIKAR V P, HARMON S M, TABAK H H, BISHOP D F, GOVIND R. Studies on biosorption of zinc(II) and copper(II) on *Desulfovibrio desulfuricans* [J]. International Biodeterioration & Biodegradation, 2000, 46: 11−18.
[50] WANG Yang-gang, LI Hao-yang, YUAN Xiao-yan, JIANG Yan-bin, XIAO Zi-an, LI Zhou. Review of copper and copper alloys as immune and antibacterial element [J]. Transactions of Nonferrous Metals Society of China, 2022, 32: 3163−3181.
[51] LIU Shuai, GUO Han-ji. A short review of antibacterial Cu-bearing stainless steel: Antibacterial mechanisms, corrosion resistance, and novel preparation techniques [J]. Journal of Iron and Steel Research International, 2024, 31: 24−45.

硫酸盐还原菌对紫铜和黄铜腐蚀的影响

徐舒华[1]，王 琴[1]，谭卓伟[1]，周小包[1]，李 聪[1]，王振生[2]，吴堂清[1]

1. 湘潭大学 材料科学与工程学院，湘潭 411105；
2. 湖南科技大学 机电工程学院，湘潭 411105

摘 要：采用微观表征和电化学方法，系统研究硫酸盐还原菌(SRB)对 H70 和 H80 黄铜及对 T2 紫铜腐蚀的影响。结果表明，无菌环境中 T2 紫铜、H70 和 H80 黄铜均表现出较优的耐蚀性能，主要腐蚀产物为 Cu_2O、CuO 和 ZnO 等金属氧化物。SRB 新陈代谢急剧加速了 3 种铜合金的腐蚀过程，其中对 T2 紫铜的加速作用最为显著。在接菌环境中，除上述金属氧化物外，铜合金表面腐蚀产物中还存在 Cu_2S、ZnS 和 $CuSO_4$ 混合物。在该环境中，H70 和 H80 黄铜主要发生点蚀，而 T2 紫铜以均匀腐蚀和点蚀为主。该研究提高了对铜合金微生物腐蚀的认识。

关键词：紫铜；黄铜；硫酸盐还原菌；微生物腐蚀；显微组织

(Edited by Xiang-qun LI)